



# Insufficient fumarase contributes to hypertension by an imbalance of redox metabolism in Dahl salt-sensitive rats

Xuewei Zheng<sup>1</sup> · Meng Chen<sup>1</sup> · Xiaoxue Li<sup>1</sup> · Pengfei Yang<sup>1</sup> · Xinrui Zhao<sup>1</sup> · Yanan Ouyang<sup>1</sup> · Zhe Yang<sup>1</sup> · Mingyu Liang<sup>2</sup> · Entai Hou<sup>1</sup> · Zhongmin Tian<sup>1</sup>

Received: 20 March 2019 / Revised: 16 May 2019 / Accepted: 29 May 2019 / Published online: 24 June 2019  
© The Japanese Society of Hypertension 2019

## Abstract

Fumarase insufficiencies can increase reactive oxygen species (ROS). This study will further dissect the imbalance of redox metabolism and the mechanism of ROS production using proteomic technology in fumarase knockdown HK-2 cells. The contribution of fumarase was further confirmed by supplementation of fumarate and malate in Dahl salt-sensitive rats. Proteomic analysis indicated that fumarase knockdown in HK-2 cells changed the expression or activity of NADPH oxidase (NOX), mitochondrial respiratory chain Complex I and III, ATP synthase subunits, and  $\alpha$ -oxoglutarate dehydrogenase (OGDH). Meanwhile, the activities of key antioxidant enzymes, including glucose-6-phosphate dehydrogenase, 6-phosphogluconate dehydrogenase, glutathione reductase, glutathione peroxidase, and glutathione S-transferase, increased significantly. The apparent activation of antioxidant defense appeared insufficient as the glutathione and GSH/GSSG ratio were decreased significantly. Dahl salt-sensitive rats exhibited changes in redox metabolism similar to HK-2 cells with fumarase knockdown. Supplementation with fumarate and malate increased and decreased, respectively, blood pressure and H<sub>2</sub>O<sub>2</sub> and malondialdehyde in salt-sensitive rats. These results indicated that insufficient fumarase activity increased ROS by regulating NOX, Complex I and III, ATPase alpha, and OGDH and the imbalance of glutathione metabolism, which may be one of the main reasons for salt-sensitive hypertension. Malate may be a potentially effective drug for the prevention and treatment of salt-sensitive hypertension.

**Keywords** Dahl salt-sensitive rats · Fumarase · Fumarate · Reactive oxygen species

---

These authors contributed equally: Xuewei Zheng, Meng Chen

**Supplementary information** The online version of this article (<https://doi.org/10.1038/s41440-019-0290-y>) contains supplementary material, which is available to authorized users.

✉ Entai Hou  
houentai001@126.com

✉ Zhongmin Tian  
zmtian@mail.xjtu.edu.cn

<sup>1</sup> The Key Laboratory of Biomedical Information Engineering of Ministry of Education, School of Life Science and Technology, Xi'an Jiaotong University, 710049 Xi'an, China

<sup>2</sup> Center of Systems Molecular Medicine, Department of Physiology, Medical College of Wisconsin, Milwaukee, WI 53226, USA

## Introduction

Salt-sensitive hypertension, a multifactorial disease affecting nearly 15% of the world population, is a major risk factor for stroke, heart failure, and end-stage renal disease [1–3]. Dahl salt-sensitive (SS) rats, as an animal model of human SS hypertension, have been widely used to dissect the pathogenesis of this condition. SS.13<sup>BN</sup> rats were used as a normotensive control, and chromosome 13 of the Brown Norway rat was integrated into the genetic background of the SS and resulted in a significant reduction in blood pressure and renal injury [4], which tremendously narrowed the pool of genes of interest on chromosome 13. There is only a 1.95% allelic difference over the entire genome between SS and SS.13<sup>BN</sup> rats. Meanwhile, SS rats' renal medulla exhibited obvious oxidative stress and blood pressure salt sensitivity compared with SS.13<sup>BN</sup> rats [5], as H<sub>2</sub>O<sub>2</sub> concentrations were also nearly twice as high in the dialysate of SS rats when both rats were maintained on a 0.4% NaCl diet [6]. The level was more than doubled with

4% NaCl in the diet, but it remained significantly higher in SS rats [6]. Furthermore, the increased production of  $O_2^-$  in medullary thick ascending limb (mTAL) of Henle's loop could also diffuse to the surrounding vasa recta, contribute to decreased bioavailability of NO and reduce medullary blood flow, resulting in sustained hypertension in SS rats [7]. However, the mechanisms of the excessive  $O_2^-$  and  $H_2O_2$  in the renal medulla of SS rats are not yet fully understood.

Our previous differential proteomics study found that fumarase (FH), the gene of which is located on rat chromosome 13, was expressed differentially between SS and SS.13<sup>BN</sup> rats, and the activity of FH was significantly lower in SS rats [8, 9]. As FH catalyzes the conversion between fumarate and L-malate, the insufficiency of FH activity in SS rat kidney was associated with increased levels of fumarate [9]. The intravenous infusion of the fumarate precursor diethyl-fumarate in SS.13<sup>BN</sup> rats resulted in increased levels of fumarate in the renal medulla and significantly exacerbated salt-induced hypertension in SS.13<sup>BN</sup> rats. Furthermore, excessive fumarate could increase the level of  $H_2O_2$  in vivo and in cultured HK-2 cells [9]. Our recent study further demonstrated that overexpressing FH on the background of the SS rat, which yielded SS-TgFh1 transgenic rats, could significantly attenuate hypertension and  $H_2O_2$  production [10]. Therefore, the present study will further dissect the mechanism of ROS production by proteomic analysis in Fh knockdown HK-2 cells.

## Materials and methods

### Cell culture and siRNA-mediated RNA interference

HK-2, a human kidney epithelial cell line, was obtained from and cultured as suggested by the Conservation Genetics CAS Kunming Cell Bank (China). RNA interference was performed as described previously [8, 11]. The small interfering RNA (siRNA) for human FH targets the CCAGGAUUAUGGUCUUGAUTT sequence (Gene Pharma Technologies, China). Scramble siRNA targeting FH that had no sequence homology with any mammalian genes was used as a negative control (NC). Each treatment had three replicates. Western blot and enzyme activity analyses were performed 64 h after transfection.

### Western blotting

Western blot was performed as described previously [12]. Sources and dilutions of primary antibodies used were FH (FH, CST, USA 1:1000); Superoxide dismutase (Mn, SOD2, Wanleibio, China, 1:2000); NADP<sup>+</sup>-dependent isocitrate dehydrogenase (cytoplasmic, NADP<sup>+</sup>-IDH1,

Wanleibio, China, 1:2000); NADP<sup>+</sup>-dependent isocitrate dehydrogenase (mitochondrial, NADP<sup>+</sup>-IDH2, BOSTER, China, 1:2000); Heat shock protein HSP 90 (HSP90, Wanleibio, China, 1:2000); 2-Oxoglutarate dehydrogenase (OGDH, CST, USA, 1:1000); ATP synthase subunit alpha (ATP5A1, Proteintech, USA, 1:2000);  $\beta$ -Actin (CW0096, China, 1:10000). Secondary antibodies were HRP-conjugated goat anti-mouse IgG (BOSTER, China) or HRP-conjugated goat anti-rabbit IgG antibody (Santa Cruz, USA). Signals were developed with a Thermo Super Signal West Pico Trial Kit. The intensities of the target proteins were quantified using ImageJ software, and  $\beta$ -actin was used as a loading control.

### Measurement of ROS and $H_2O_2$

ROS levels were detected using dichlorodihydrofluorescein diacetate ( $H_2DCF$ -DA) (Sigma-Aldrich) [13]. Fluorescence was determined with a fluorescence spectrometer (TECAN Infinite M200 PRO, Schweiz) at 485 nm (excitation) and 538 nm (emission). Cellular oxidant levels were expressed as relative DCF fluorescence per sample protein amounts (measured using a BCA assay).  $H_2O_2$  generation was detected using a Hydrogen Peroxide assay kit (Jiancheng Biochemical).

### Proteomic analysis

#### Protein reduction, cysteine block, and digestion

HK-2 cells were lysed in a buffer containing 8 mol/L urea, 4% CHAPS, 1% DTT, and 1% IPG buffer (GE Healthcare) at 4 °C for 1 h. The cell lysates were centrifuged at 15,000 g for 25 min. The supernatant was collected, and the protein concentration was determined by the Bradford method [14]. A volume corresponding to 100  $\mu$ g of protein was precipitated with 5 volumes of acetone at -20 °C for 1 h. After centrifugation for 10 min at 15,000 g, the deposits were collected and dried by a vacuum freezing dryer. Then, the protein pellets were dissolved in 50  $\mu$ L iTRAQ dissolution buffer (Applied Biosystems), and 4  $\mu$ L reducing reagent (Applied Biosystems) was added at 60 °C for 1 h. After cooling samples to room temperature (RT), cysteine residues were blocked with 2  $\mu$ L 200 mmol/L methyl methane thiosulfate by incubating at RT for 10 min. The protein solutions were added to 10 kDa ultrafiltration tubes and cleaned by centrifugation (12,000 rpm, 20 min). Then, 100  $\mu$ L of iTRAQ dissolution buffer was added to ultrafiltration tubes, centrifuged at 12,000 g for 15 min and repeated three times. The column was placed in a new tube, 50  $\mu$ L sequencing-grade trypsin (50 ng/ $\mu$ L) was added, and the sample was incubated at 37 °C for 12 h. Afterward, the peptide was centrifuged at 12,000 g for 20 min, and the

peptide was collected. The filter units were transferred to a new collection tube, and 50  $\mu\text{L}$  of iTRAQ dissolution buffers was added to centrifuge the tube again. The two filter solutions were combined.

Protein digestion and labeling with iTRAQ reagents. The labeling reactions were performed following the manufacturer's recommendations. Peptide samples from negative control HK-2 cells were labeled with iTRAQ reagent, and 113 isobaric tag and peptide samples from FH siRNA-treated HK-2 cells were labeled by adding the same amount of iTRAQ reagent, 114 isobaric tag. After 2 h of incubation at RT, reactions were stopped by adding 100  $\mu\text{L}$  of water to each vial.

### Peptide fractionation by strong cation exchange chromatography

The mixed peptides were fractionated by strong cation exchange chromatography. Samples were separated using an Agilent 1200 HPLC System (Agilent), Michrom column (Poly-SEA 5  $\mu\text{m}$  300  $\text{\AA}$  2.0  $\times$  150 mm) at a flow rate of 0.3 mL/min, using a nonlinear binary gradient starting with buffer A (10 mmol/L formic acid, 20% acetonitrile) and transitioning to buffer B (500 mmol/L formic acid, 20% acetonitrile). First, the column was washed with buffer A for 5 min, and peptides were eluted with a four-step gradient: first, a linear gradient of 5–50% buffer B for 25 min, followed by a linear gradient of 50–80% buffer B for 5 min. The gradient was ramped to 100% buffer B in 1 min and held for 10 min. The first fraction from 0 to 5 min was collected, then, each fraction was collected with a 4-min interval for the 6–44 min, and the last fraction was from 45 to 50 min, with a total of 12 segments. Each fraction was dried in a vacuum freezing dryer for LC-MS/MS analysis.

### RPLC-MS/MS analysis

The online Nano-RPLC was employed on the Eksigent nanoLC-Ultra™ 2D System (AB SCIEX). The samples were loaded onto a C<sub>18</sub> nano LC trap column (100  $\mu\text{m}$   $\times$  3 cm, C<sub>18</sub>, 3  $\mu\text{m}$ , 150  $\text{\AA}$ ) and washed with Nano-RPLC buffer A (0.1% formic acid, 2% acetonitrile) at 2  $\mu\text{L}/\text{min}$  for 10 min. An elution gradient of 5–35% acetonitrile (0.1% formic acid) in a 70 min gradient was used on an analytical Chrom XP C<sub>18</sub> column (75  $\mu\text{m}$   $\times$  15 cm, C<sub>18</sub>, 3  $\mu\text{m}$ , 120  $\text{\AA}$ ) with a spray tip. Data acquisition was performed with a Triple TOF 5600 System (AB SCIEX, USA) fitted with a Nanospray III source (AB SCIEX, USA) and a pulled quartz tip as the emitter (New Objectives, USA). Data were acquired using an ion spray voltage of 2.5 kV, curtain gas of 30 PSI, nebulizer gas of 5 PSI, and an interface heater temperature of 150 °C. For information-dependent acquisition, survey scans were acquired in 250 ms, and as many as

35 product ion scans were collected if they exceeded a threshold of 150 counts/s with a 2<sup>+</sup> to 5<sup>+</sup> charge-state. The total cycle time was fixed to 2.5 s. A rolling collision energy setting was applied to all precursor ions for collision-induced dissociation. Dynamic exclusion was set for 1/2 of peak width (18 s), and the precursor was then refreshed off the exclusion list.

### Protein identification and quantification

Data were processed with Protein Pilot Software v. 4.0 (AB SCIEX, USA) against the Homo sapiens database using the Paragon algorithm [15]. Protein identification was performed with the search option: emphasis on biological modifications. The database search parameters were as follows: instrument was Triple TOF 5600, iTRAQ 2-plex quantification, cysteine modified with iodoacetamide, and biological modifications were selected as the ID focus, trypsin digestion. An automatic decoy database search strategy was employed to estimate the false discovery rate (FDR) using the PSPEP (Proteomics System Performance Evaluation Pipeline Software, integrated in the Protein Pilot Software). The FDR was calculated as the false positive matches divided by the total matches. The iTRAQ 2-plex was chosen for protein quantification with unique peptides during the search.

### GO and KEGG pathway enrichment analysis

The multiomics data analysis tool Omics Bean was used to analyze the obtained proteomics data (<http://www.omicsbean.com:88>), in which distributions in biological functions, subcellular locations, and molecular functions (MFs) were assigned to each protein based on Gene Ontology (GO) categories. The Kyoto Encyclopedia of Genes and Genomes (KEGG) pathway analysis was performed to enrich high-level functions in the defined biological systems.

### Enzymes activity assays

The obtained pellets were lysed by three freeze–thaw cycles to ensure that the mitochondrial membrane was disrupted and enzymes were accessible. The protein content was determined with a BCA protein assay kit (Beyotime Institute of Biotechnology, China).

The enzyme activity of FH was measured based on a previously reported method [9]. The activities of glutathione reductase (GR) were assayed using Beyotime Detection kits (Beyotime Institute of Biotechnology, China) according to the corresponding protocols. The activities of glutathione S-transferase (GST) and glutathione peroxidase (GPx) in HK-2 cells were assayed using the Jiancheng Biochemical detection kits. Glucose-6-phosphate dehydrogenase (G6PD) and

6-phosphogluconate dehydrogenase (6PGD) activities were assessed as described previously [16, 17]. The activities of isocitrate dehydrogenase, NADP<sup>+</sup>-IDH1 (cytoplasmic) and NADP<sup>+</sup>-IDH2 (mitochondrial) were assayed by spectrophotometric monitoring of the reduction of NADP<sup>+</sup> to NADPH at 340 nm according to protocol by Yarian [18]. The NADPH oxidase (NOX) activity was determined using the NADPH oxidase assay kit purchased from Nanjing Jiangcheng Bioengineering Institute.

### GSH/GSSG and NADPH/NADP<sup>+</sup> measurements

The analyses of reduced glutathione (GSH) and oxidized glutathione (GSSG) were performed using the DTNB method with kits according to the corresponding kit protocols (Beyotime, China). The NADP<sup>+</sup> and NADPH analyses were performed with kits according to the corresponding kit protocols (Comin, China).

### GC/MS assay

The extraction of metabolites in tissue and cell samples was performed according to the method described in previous reports [19, 20]. Dried tissue and cell residues were derivatized using a two-step procedure with a minor modification [21, 22]. For oximation, 80  $\mu$ L of 10 mg/mL methoxyamine hydrochloride (Sigma-Aldrich) dissolved in pyridine was mixed with a lyophilized sample and kept at 30 °C for 90 min. Then, 80  $\mu$ L of N,O-bis(trimethylsilyl)-trifluoroacetamide (BSTFA) with 1% TMCS (Sigma-Aldrich) was added for derivatization and heated to 70 °C for 60 min. GC/MS analysis was performed according to our previous report [22], using a 7890 A /5975 C Inert MSD (Agilent Technologies, Wilmington, DE) coupled with a DB-5 column (30 m  $\times$  0.25 mm I.D.; film thickness: 0.25  $\mu$ m; Agilent J&W Scientific, USA). Helium was used as the carrier gas at a constant flow rate of 1 mL/min. The GC temperature programming was set to 2 min isothermal heating at 80 °C, followed by 10 °C/min in an oven with temperature ramps to 120 °C and 5 °C/min to 260 °C and then increases at a rate of 10 °C/min to 300 °C, where it was held for 2 min. Fumarate, L-malate, glutamate, glycine, and L-cysteine standards were analyzed under identical experimental conditions for further identification. One microliter of the final derivatized aliquots was injected into the GC/MS.

### Measurement of ATP

The ATP assay was performed with a kit from Promega (G7570). The luminescence was recorded in a TECAN Infinite M200 PRO (Schweiz) with an integration time of 5 s per well.

### Animals and tissues

Male SS rats (SS/JrHsdMcwi) and consomic, salt-insensitive SS.13<sup>BN</sup> rats [4] were bred in a pathogen-free animal house and maintained on a purified AIN-76A rodent diet containing 0.4% NaCl with free access to water. For tissue collection, kidneys were flushed in situ with cold saline, and the renal cortex and medulla were quickly removed and snap-frozen in liquid nitrogen and stored at -80 °C. Frozen tissues were used for preparation of tissue homogenates to perform activity assays, western blots, and metabolite analysis. The experiments were approved by the Institutional Animal Ethics Committee of Xi'an Jiaotong University.

### Fumarate and malate supplementation

Male SS rats were fed a 0.4% NaCl diet since weaning. After 3 days of stable baseline blood pressure at ~7 weeks of age, rats were switched to an 8% NaCl diet (HS). Fumarate (50 mg/kg/d) [23], malate (600 mg/kg/d) [24], or an equal volume of distilled water was delivered by gavage. Serum and kidneys were harvested at the end of blood pressure measurement on day 17 of the HS diet.

### Measurement of blood pressure

The blood pressure of conscious rats was measured using tail-cuff plethysmography with a CODA-4 computerized system (Kent Scientific Corporation, Torrington, Connecticut, USA). Mean arterial pressure (MAP) was measured between 14:00 and 16:00 by a single experienced operator. Rats were trained for the procedure for 5 consecutive days. After calibrating the tail-cuff apparatus, rats were placed on the platform and allowed to rest in a glass restrainer. A black conical plastic piece with a nose opening was placed over the head region of the rat to cover the eyes and allow the rat to rest. The platform was heated to 30–32 °C to increase the detection of the oscillation waveforms generated by the blood flow in the tail. Each session was composed of 15 successive measurements of the systolic and diastolic pressure, which were averaged. The heart rate was recorded at the same time.

### Measurement of H<sub>2</sub>O<sub>2</sub> and MDA in the kidneys of SS rats

H<sub>2</sub>O<sub>2</sub> and malondialdehyde (MDA) generation were detected using a Hydrogen Peroxide assay kit (Jiancheng Biochemical).

### Statistical analysis

All values are presented as the mean  $\pm$  SEM. All data were analyzed using Student's *t*-test or ANOVA. *P* < 0.05 was

considered statistically significant. All statistical tests were performed with GraphPad Prism software, version 6.0 (Graph Pad Software Inc., San Diego, CA).

## Results

### Differentially expressed proteins between FH-insufficient HK-2 cells and NC cells

FH was knocked down by siRNA in HK-2 cells, the protein profile of the whole cells was analyzed by iTRAQ-based proteomics technology, and metabolites were detected by GC/MS. The content and activity of FH were examined to ensure the efficiency of FH knockdown. The sample preparation used for proteomic analysis was the same as the description we reported [25], and the sample test is shown in Supplementary Fig. 1.

A total of 3174 proteins were identified in HK-2 cells, with the value of the global FDR less than 1%, and those identified with more than two peptides for 95% confidence were considered for further analysis (Supplementary Table 1). Proteins with a fold change of  $>1.50$  or  $<0.67$  were considered to be significantly differentially expressed (Supplementary Table 1). Compared with the NC cells, 267 identified proteins exhibited significant differences in Fh knockdown HK-2 cells (fold change  $>1.5$ ,  $P < 0.05$ ) (Supplementary Table 2). Among them, 165 proteins were upregulated and 102 proteins were downregulated compared to NC. In addition, SOD2, IDH1, IDH2, and HSP90 among the 267 differentially expressed proteins were further confirmed by western blotting. As shown in Supplementary Fig. 2, the relative protein content from western blotting was consistent with proteomic quantification.

### GO and KEGG analysis of the differentially expressed proteins

To clarify the changed metabolic pathways involved in the response to Fh knockdown, 267 differentially expressed proteins were further examined using the Omics Bean bioinformatics tool. (GO enrichment analysis was conducted in the biological process (BP), cellular component (CC), and MF categories. An overview of significantly changed proteins in the BP, CC, and MF categories is shown in Supplementary Fig. 3 and Supplementary Table 3. KEGG pathway-based analysis showed that ribosome, carbon metabolism, glutathione metabolism, mRNA transport, pyruvate metabolism, fatty acid degradation, glycolysis/gluconeogenesis, and TCA cycle were significantly enriched among 267 differential proteins (Supplementary Fig. 4 and Supplementary Table 4).

### The generation sites of excessive amounts of ROS and H<sub>2</sub>O<sub>2</sub> in Fh knockdown HK-2 cells

NOX activity was detected and significantly increased in Fh knockdown HK-2 cells compared with NC cells (Fig. 1a). The differential proteomic analysis data showed that expression of NADH dehydrogenase (ubiquinone) iron–sulfur protein 5 (NDUFS5), subunit of respiratory chain Complex I, Rieske iron–sulfur protein (RISP), and Cyt b-c1 Complex subunit 6 (Complex III) was reduced by 1.5 times in Fh knockdown HK-2 cells. Meanwhile, the expression of OGDH and cytochrome b5 reductase (B5R) increased by 1.5 and 1.7 times. Except for these defined ROS generation sites, the F<sub>1</sub>F<sub>0</sub> ATP synthase subunits ATP5A1, ATP5C1, ATP5I, and ATP5L were reduced by 1.7, 1.4, 1.5, and 2.1 times (Supplementary Table 2), and ATP levels were significantly reduced (Fig. 1c). Briefly, NOX,  $\alpha$ -OGDH, B5R, ATPase, and Complex I and III would be the main sites of ROS formation in Fh knockdown HK-2 cells.

### Glutathione metabolism and antioxidant systems in Fh knockdown HK-2 cells

The redox state of the cell is finely regulated by antioxidant systems, which include antioxidant enzymes and small molecular weight antioxidants. The proteomic analysis identified the expression of all key enzymes involved in glutathione metabolism and increased their protein expression, including GPx, GR, GST, glutathione synthetase (GS), G6PD, and 6PGD (Supplementary Table 1). Meanwhile, the activities of G6PD, 6PGD, GR, GST, and GPx also increased compared with NC cells (Fig. 1b, d–f). In contrast, there was no significant difference in the expression of glutamate cysteine ligase. In addition, the expression of other antioxidant enzymes, SOD2, nicotinamide nucleotide transhydrogenase (NNTH), and IDH2 increased by 1.69, 1.77, and 1.43 times; however, CAT and SOD1 showed no significant difference between Fh knockdown HK-2 cells and NC cells (Supplementary Table 1). The expression of SOD2, IDH1, and IDH2 was further confirmed by western blotting (Supplementary Fig. 2). Furthermore, the expression of L-lactate dehydrogenase (LDHB), NADPH-dependent alcohol dehydrogenase (AKR1A1), glutathione dependent formaldehyde dehydrogenase (ADH5), and L-glutamate gamma semialdehyde dehydrogenase (ALDH7A1) increased by 1.7, 1.5, 1.5, and 1.4 times compared with NC cells (Supplementary Table 1). These data suggested that the increased activity of dehydrogenase would supply more antioxidants, such as GSH, NADH, or NADPH. Unfortunately, the GSH content decreased dramatically, especially when the GSH/GSSG ratio decreased, even when the NADPH content increased compared with NC cells. The GSH synthesis substrates glutamate, glycine, and L-cysteine were also significantly reduced (Fig. 2a–f).

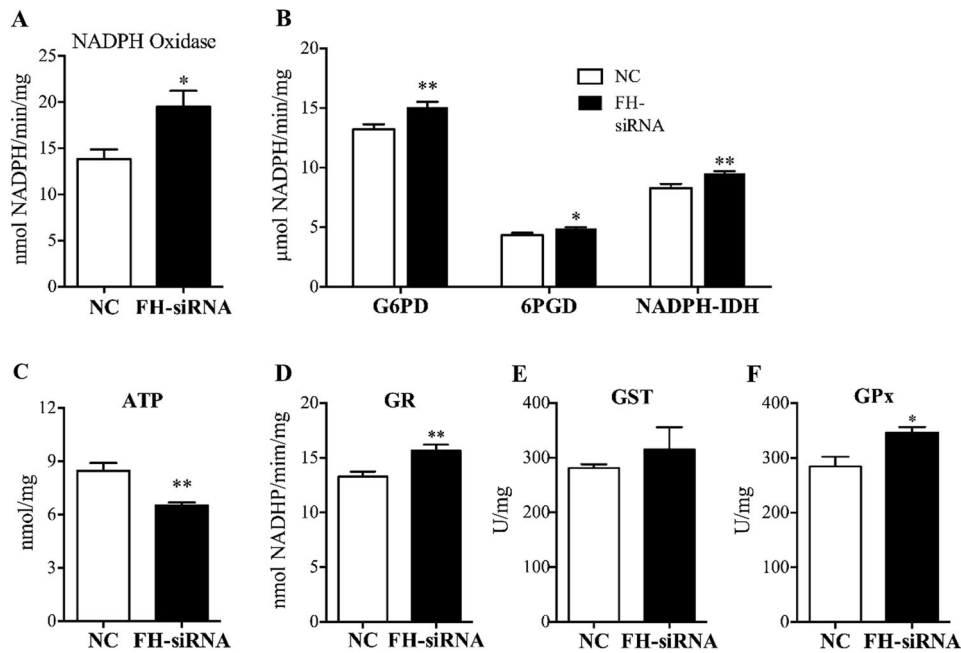


**Fig. 1** NADPH oxidase and key enzymes involved in glutathione metabolism activities in FH-insufficient HK-2 cells. **a** NADPH oxidase activity was enhanced in FH-insufficient HK-2 cells. **b** Fumarase insufficiency attenuated ATP production. **c** Glucose-6-phosphate 1-dehydrogenase (G6PD), 6-phosphogluconate dehydrogenase (6PGD), and NADP<sup>+</sup>-IDH activity. **d** Glutathione reductase (GR) activity.

**e** Glutathione S-transferase (GST) activity. **f** Glutathione peroxidase (GPx) activity. Scramble siRNA targeting FH that had no sequence homology with any mammalian genes as a negative control (NC). Data are presented as the mean value  $\pm$  SEM,  $n = 4$ , \* $p < 0.05$ , \*\* $p < 0.01$  compared to NC cells

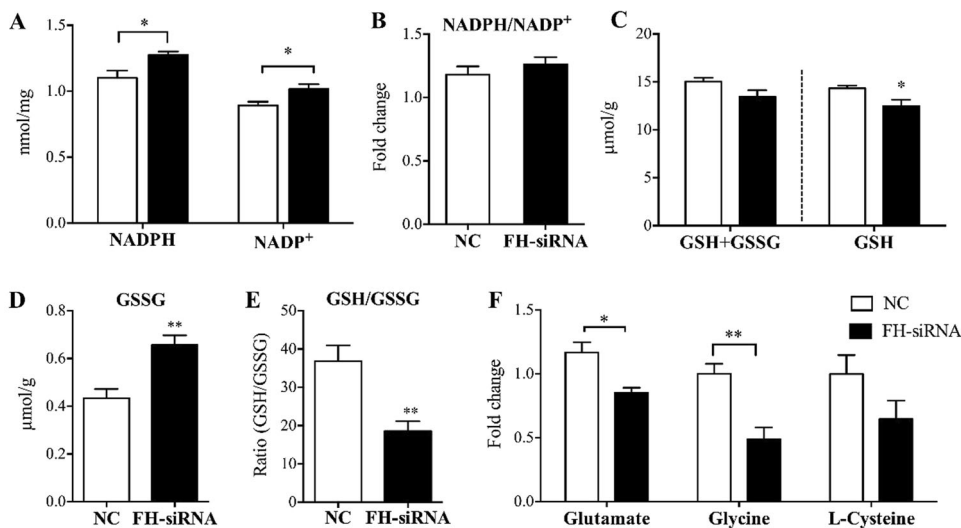


**Fig. 2** Fumarase insufficiency is associated with increased NADPH, NADP<sup>+</sup> and reduced total GSH and GSH/GSSG ratio. **a** NADPH and NADP<sup>+</sup> levels were detected in negative control and FH insufficient HK-2 cells. **b** NADPH/NADP<sup>+</sup> ratio. **c** Total GSH (GSH + GSSH) and GSH levels. **d** GSSG levels. **e** GSH/GSSG ratio. **f** Fold changes of

the glutamate, glycine, and L-cysteine levels in FH-insufficient HK-2 cells were calculated as a ratio relative to the negative control. Scramble siRNA targeting FH had no sequence homology with any mammalian genes as a negative control. Data are presented as the mean value  $\pm$  SEM,  $n = 6$ , \* $p < 0.05$ , \*\* $p < 0.01$  compared to NC cells

### Key enzymes involved in renal redox metabolism of Dahl SS rats

The FH activity was insufficient in the renal cortex and medulla of SS rats compared with SS.13<sup>BN</sup>. To confirm that

the renal cells exhibited the same response to insufficient FH activity as Fh knockdown HK-2 cells, the expression and activity of these key enzymes involved in redox metabolism were detected. For ROS formation, the activity of NOX had been reported to increase definitely in the renal

**Fig. 3** Western blot analysis of protein abundance of OGDH and ATP5A1 in the kidneys of SS and SS.13<sup>BN</sup> rats.

**a** Abundance of  $\alpha$ -oxoglutarate dehydrogenase (OGDH) and ATP synthase subunit alpha (ATP5A1) in the renal cortex. **b** Abundance of OGDH and ATP5A1 in the renal medulla.  $\beta$ -actin was used as the internal loading control. Data are presented as the mean value  $\pm$  SEM,  $n = 4$ ,  $*p < 0.05$  compared to the negative control

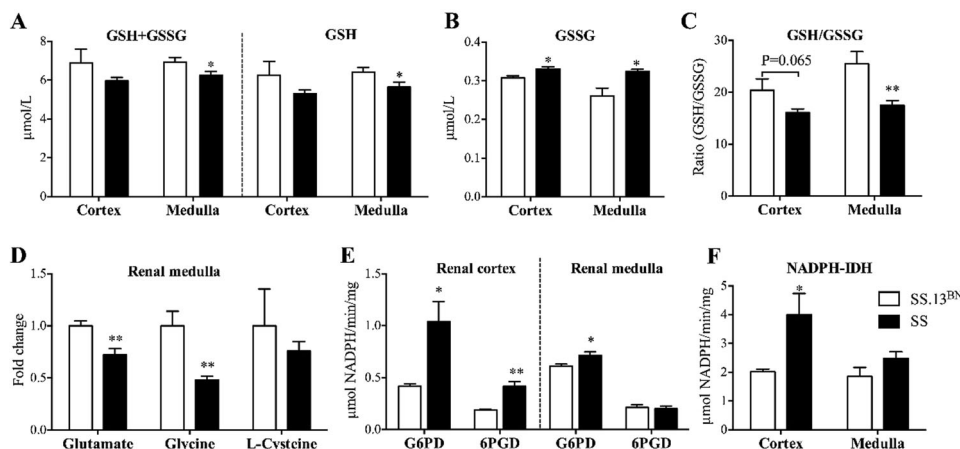
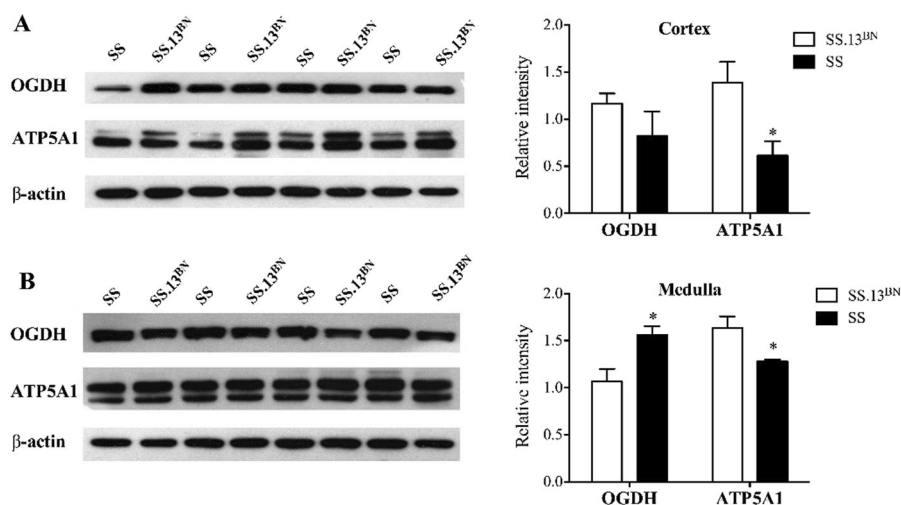


**Fig. 4** Total GSH levels and GSH/GSSG ratio were reduced in the kidney of SS rats. **a** Total GSH (GSH + GSSG) and GSH levels were reduced in the renal cortex and medulla. **b** GSSG levels. **c** GSH/GSSG ratio. **d** Fold changes of glutamate, glycine, and L-cysteine in the renal

medulla. **e** G6PD and 6PGD activity in the renal cortex and medulla. **f** NADPH<sup>+</sup>-IDH activity in the renal cortex and medulla. Data are presented as the mean value  $\pm$  SEM,  $n = 5$ ,  $*p < 0.05$  compared to the negative control

medulla of SS rats [5], similar to Fh knockdown HK-2 cells. The expression of OGDH increased significantly, and the expression of ATP5A1 was reduced significantly in the renal medulla (Fig. 3a, b). SS rat mitochondrial respiratory chain Complexes I and III have been reported to be involved in ROS production due to the insufficient expression of elongation factor Tu protein in the mTAL mitochondria [26].

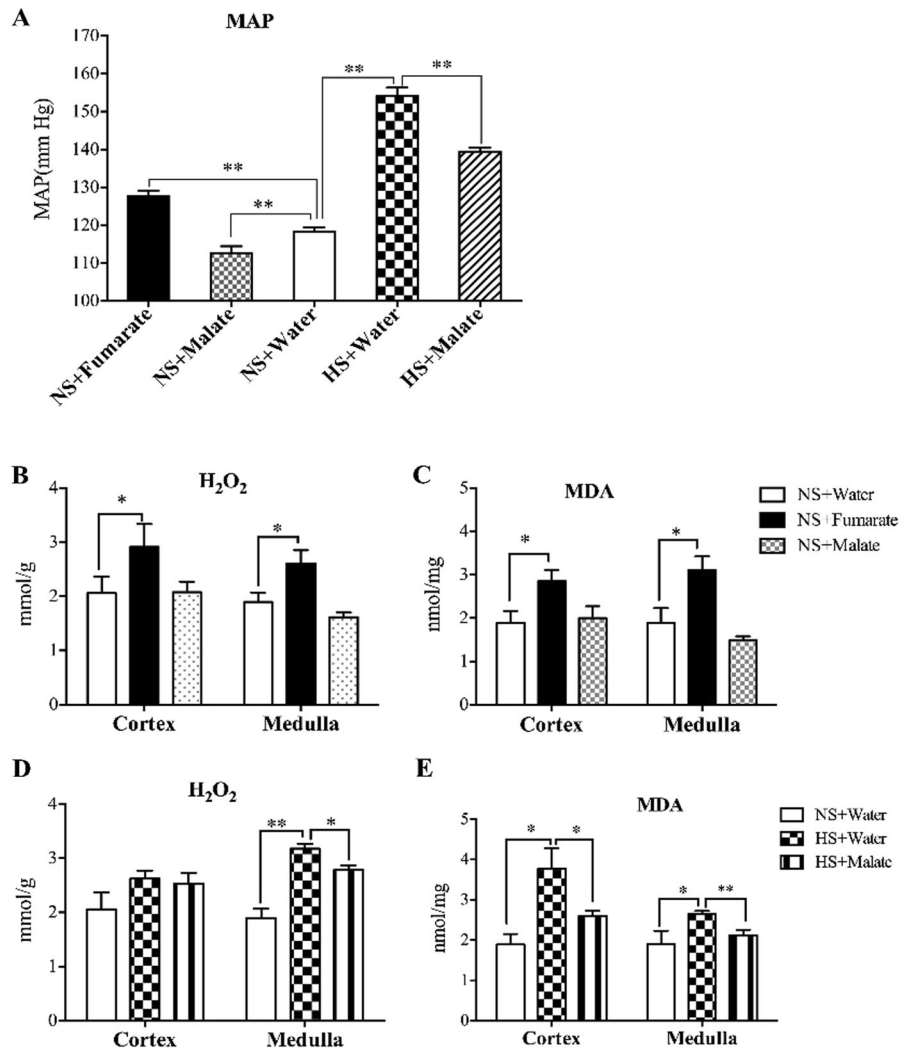
For the antioxidant response, the total GSH (GSH + GSSG) and GSH were significantly reduced in the renal medulla (Fig. 4a). The GSSG increased both in the renal cortex and medulla (Fig. 4b). The ratio of GSH/GSSG was significantly reduced in the renal medulla ( $P < 0.01$ ) and renal cortex ( $P = 0.065$ ) (Fig. 4c). The GSH synthesis substrates glutamate, glycine, and L-cysteine were reduced significantly in the renal medulla (Fig. 4d). Meanwhile, the

activity of G6PD increased in the renal cortex and medulla, but the activity of 6PGD and NADPH<sup>+</sup>-IDH only increased in the renal cortex of SS rats compared with SS.13<sup>BN</sup> rats (Fig. 4e, f). These data suggested that the renal tissue of SS rats had similar redox metabolism to Fh knockdown HK-2 cells.

### Redox state in kidneys of SS rats orally administered fumarate and malate

The insufficiency of FH activity will result in the accumulation of fumarate and a slight insufficiency of malate. As FH is not directly involved in the formation of ROS, the metabolic intermediate fumarate or malate likely participates in ROS production. To further verify the contribution of fumarate and malate to ROS generation, malate and

**Fig. 5** Levels of  $H_2O_2$  and MAD in the kidneys of SS rats with fumarate or malate supplementation. **a** Mean arterial blood pressure (MAP) of SS rats on a 0.4% salt (normal salt, NS) diet with or without malate (fumarate) or an 8% salt (high salt, HS) diet with or without malate supplementation by gavage. **b** Levels of  $H_2O_2$  in the renal cortex and medulla of SS rats on 0.4% salt with or without malate (fumarate) supplementation by gavage. **c** Levels of MDA in the renal cortex and medulla of SS rats on 0.4% salt with or without malate (fumarate) supplementation by gavage. **d** Levels of  $H_2O_2$  in the renal cortex and medulla of SS rats on a 0.4% salt or 8% salt diet with or without malate supplementation by gavage. **e** Levels of MDA in the renal cortex and medulla of SS rats on a 0.4% salt or 8% salt diet with or without malate supplementation by gavage. Data are presented as the mean value  $\pm$  SEM.  $n = 5-6$ ,  $*p < 0.05$ ,  $**p < 0.01$



fumarate were delivered by gavage in SS rats fed a normal salt diet and a high salt diet. The levels of  $H_2O_2$  and MDA were detected after malate and fumarate supplementation for 2 weeks. The results showed that the levels of  $H_2O_2$  and MDA increased significantly in the renal cortex and medulla of SS rats with fumarate oral administration, while the blood pressure increased significantly (Fig. 5a). In contrast, oral administration of malate did not influence the levels of  $H_2O_2$  and MDA in SS rats fed a normal salt diet, and the blood pressure was significantly reduced (Fig. 5b, c). When SS rats were fed a high salt diet for 2 weeks, the levels of  $H_2O_2$  and MDA increased dramatically in the renal medulla, and the oral administration of malate significantly attenuated the increases in  $H_2O_2$ , MDA, and blood pressure caused by the high salt diet (Fig. 5d–e). These data demonstrated that the substrate of FH, fumarate, could exacerbate ROS production and hypertension in SS rats; in contrast, the product of FH, L-malate, could attenuate the hypertension induced by a high salt diet.

## Discussion

### Imbalance of the redox state in Fh knockdown HK-2 cells

GST catalyzes the conjugation of the reduced form of GSH to xenobiotic substrates and plays an important role in cellular defense against oxidative stress and toxic electrophile species that arise through normal metabolic processes [27]. The upregulated expression and improved activity of GPx and GST suggested excessive consumption of GSH after Fh knockdown.

GR catalyzes the reduction of GSSG to the sulfhydryl form GSH via the conversion of NADPH to  $NADP^+$ , which is a critical molecule in resisting oxidative stress and maintaining the reducing environment of the cell. The main source of NADPH in the cell is the pentose phosphate pathway (PPP), in which G6PD and 6PGD were defined as the rate-limiting enzymes. The activity of GR, G6PD, and



6PGD was increased significantly in response to Fh knockdown in HK-2 cells (Fig. 1). This result was also consistent with the increased protein expression. In addition to PPP, NADPH can be produced from other oxidoreductases, such as IDH2, which oxidizes a substrate by reducing an electron acceptor, usually  $\text{NAD}^+$  or  $\text{NADP}^+$ , and producing NADH or NADPH. Indeed, the activity of  $\text{NADP}^+$ -IDH2 increased significantly (Fig. 1c). Meanwhile, the expression of other dehydrogenases, such as LDHB, AKR1A1, ADH5, and ALDH7A1, also increased significantly in Fh knockdown cells. These data suggested that increasing the expression of dehydrogenase could provide more NADPH or NADH for the consumption of GR. In addition, the oxidation of NADPH through mitochondrial electron transfer chains was decreased because adrenodoxin oxidoreductase (FDXR), serving as the first electron transfer protein in all mitochondrial P450 systems, was reduced by 1.77-fold. The ratio of  $\text{NADPH}/\text{NADP}^+$  slightly increased (Fig. 2b).

As all key enzymes (GR, GS, GST, GPx, G6PD, and 6PGD) involved in glutathione metabolism increased their activities or protein expression, the oxidation-reduction reaction that GSH participated in was extremely active in HK-2 cells after Fh knockdown.

The ratio of GSH/GSSG is often used as an indicator of the cellular redox state since it is the most abundant thiol-disulfide redox buffer in the cell [28]. Normally, GSH is approximately 30- to 100-fold higher than GSSG. The oxidation of only a small amount of GSH to GSSG can significantly change the ratio and the redox status of the cell. However, knockdown of FH expression resulted in a significant decrease of GSH/GSSG in HK-2 cells (Fig. 2e). The results further confirmed that insufficient FH activity could result in oxidative stress. Nevertheless, where did these ROS come from?

The activity of NOXs was detected and showed a significant increase in Fh knockdown HK-2 cells, which should contribute to ROS production (Fig. 1a). Mitochondrial enzymes are so far known to generate ROS, including the TCA cycle enzymes aconitase (ACO), OGDH, PDH, glycerol-3-phosphate dehydrogenase (GPDH), B5R, and Complexes I, II, and III [29]. Current differential proteomics analysis data showed that the expression of NDUF55, an important member of Complex I, was significantly reduced. Its expression modulates the efficiency of the mitochondrial electron transport chain and ATP level [30]. The full assembly of Complex I will be disturbed by insufficient expression of NDUF55, and ROS generation will be promoted [31, 32]. RISP is one of the catalytic subunits of Complex III, and it has been demonstrated that RISP deficiency influences the stability of Complex I and Complex III and increases the generation of ROS [33]. Both RISP and Cyt b-c1 Complex subunit 6 were reduced 1.5-fold in Fh knockdown HK-2 cells. This result suggested that

Complex III contributed to the production of ROS. Meanwhile, the upregulation of both OGDH and B5R also promoted ROS production. ATP synthase has been defined as one important site of ROS generation. Its activity can modulate ROS formation and ATP levels in mitochondria [34]. ATP5A1 was identified as a target for calpain-1 in diabetic hearts, leading to its proteolytic degradation. The disruption of ATP5A1 may compromise mitochondrial function, resulting in excessive ROS generation in mice [35]. Current data showed that the expression of the ATP synthase subunits ATP5A1, ATP5C1, ATP5I, and ATP5L was significantly reduced, and accordingly, ATP levels were reduced (Fig. 1b).

Briefly, the signature of redox metabolism for Fh knockdown HK-2 cells would be NOX,  $\alpha$ -OGDH, B5R, ATPase, and Complex I and III as the main sites of ROS formation, and upregulated expression of GR, GS, GST, GPx, G6PD, 6PGD, SOD2, IDH2, and NNTH was an antagonistic response to the excessive ROS. The final substantial drop in GSH/GSSG ratio was the result of Fh knockdown. The redox metabolism of Fh knockdown HK-2 cells is summarized in Supplementary Fig. 5.

### Oxidative stress in the renal medulla and cortex of SS rats

NOX was the major source of excess superoxide produced in the renal medulla of SS rats [5]. The increase of NOX activity is consistent with it in Fh knockdown HK-2 cells. The expression of OGDH increased in the renal medulla, whereas the expression of ATP5A1 was significantly reduced in the renal medulla and cortex of SS rats compared with SS.13<sup>BN</sup>. These results suggest that OGDH and ATPase may also contribute to ROS formation in the renal medulla of Dahl SS rats. Meanwhile, mitochondrial proteomics analysis also suggested that Complex I and Complex III were the ROS production sites in renal mTAL of the SS rats [26]. Briefly, B5R, NOX,  $\alpha$ -OGDH, ATPase, and Complex I and III are the sites of ROS production in the renal medulla of SS rats.

For the antioxidant response of SS rats, the synthesis of GSH was also modulated by insufficient substrates, as the levels of glycine, glutamate, and cysteine were reduced in the renal medulla compared with SS.13<sup>BN</sup>. The levels of GSH, GSSG, and total GSH (GSH + GSSG) in the renal medulla of SS rats were similar to those in Fh knockdown HK-2 cells. In particular, the ratio of GSH/GSSG was also significantly reduced. GPx had been reported to increase in SS medulla [36]. Other dehydrogenases, such as IDH2, 6GPD, and G6PD, also increased their expression or activity (Fig. 4e). These enzymes in the renal medulla of SS rats had the same response to oxidative stress as Fh knockdown HK-2 cells. The full comparison involved in the

redox balance between SS rats and Fh knockdown HK-2 cells is listed in Supplementary Table 5. All the data suggested that the imbalance of redox metabolism in the renal medulla of SS rats was highly similar to Fh knockdown HK-2 cells.

### Fumarate and malate contribute to the imbalance of redox and hypertension in SS rats

There is no evidence to confirm that FH is the site of ROS production, but the excessive fumarate formed by the insufficient FH activity could lead to oxidative stress by succination of GSH [37]. This covalent adduct between fumarate and GSH reduced the efficiency and level of GSH in the cell. Meanwhile, the total GSH (GSH + GSSG) and GSH levels were significantly reduced in SS renal cells and HK-2 cells as inadequate synthetic substrates, such as glycine and glutamate. Obviously, the insufficient GSH flux attenuated the antioxidant ability of the GSH system and promoted ROS formation. Current data showed that extra fumarate oral administration significantly increased the levels of H<sub>2</sub>O<sub>2</sub> and MDA and exacerbated the elevation of MAP. As with the production of FH, excess malate oral administration could reduce the generation of ROS and attenuated the high salt diet-induced hypertension (Fig. 5). These data further demonstrated that insufficient FH activity contributed to the generation of ROS and hypertension in Dahl SS rats.

**Acknowledgements** This study was supported by the National Natural Science Foundation of China (Grant nos. 81770728, 81570655, 51703178).

**Author contributions** Z.T. and M.L. conceived the study. E.H., X.W.Z., M.C., X.L., P.Y., X.R.Z., Y.O.Y., and Z.Y. designed and developed the study. E.H. and X.W.Z. processed and analyzed the data.

### Compliance with ethical standards

**Conflict of interest** The authors declare that they have no conflict of interest.

**Publisher's note** Springer Nature remains neutral with regard to jurisdictional claims in published maps and institutional affiliations.

### References

- Kotchen TA, Cowley AW, Liang MY. Ushering hypertension into a new era of precision. *J Am Med Assoc.* 2016;315:343–4.
- Whelton PK. The elusiveness of population-wide high blood pressure. *Control Annu Rev Public Health.* 2015;36:109–30.
- Kearney PM, Whelton M, Reynolds K, Muntner P, Whelton PK, He J. Global burden of hypertension: analysis of worldwide data. *Lancet* 2005;365:217–23.
- Cowley AW, Roman RJ, Kaldunski ML, Dumas P, Dickhout JG, Greene AS, et al. Brown Norway chromosome 13 confers protection from high salt to consomic Dahl S rat. *Hypertension* 2001;37:456–61.
- Taylor NE, Glocka P, Liang M, Cowley AW Jr. NADPH oxidase in the renal medulla causes oxidative stress and contributes to salt-sensitive hypertension in Dahl S rats. *Hypertension* 2006;47:692–8.
- Taylor NE, Cowley AW Jr. Effect of renal medullary H<sub>2</sub>O<sub>2</sub> on salt-induced hypertension and renal injury. *Am J Physiol Regul, Integr Comp Physiol.* 2005;289:R1573–9.
- Cowley AW. Renal medullary oxidative stress, pressure-natriuresis, and hypertension. *Hypertension.* 2008;52:777–86.
- Tian ZM, Greene AS, Usa K, Matus IR, Bauwens J, Pietrusz JL, et al. Renal regional proteomes in young Dahl salt-sensitive rats. *Hypertension.* 2008;51:899–904.
- Tian ZM, Liu Y, Usa K, Mladinov D, Fang Y, Ding XQ, et al. A novel role of fumarate metabolism in dahl salt-sensitive hypertension. *Hypertension.* 2009;54:E63–4.
- Usa K, Liu Y, Geurts AM, Cheng Y, Lazar J, Baker MA, et al. Elevation of fumarase attenuates hypertension and can result from a nonsynonymous sequence variation or increased expression depending on rat strain. *Physiol Genom.* 2017;49:496–504.
- Liang MY, Pietrusz JL, Pietrusz L. Thiol-related genes in diabetic complications—a novel protective role for endogenous thiorodoxin 2. *Arterioscler Thromb Vasc Biol.* 2007;27:77–83.
- Feng D, Yang C, Geurts AM, Kurth T, Liang MY, Lazar J, et al. Increased expression of NAD(P)H oxidase subunit p67(phox) in the renal medulla contributes to excess oxidative stress and salt-sensitive hypertension. *Cell Metab.* 2012;15:201–8.
- Lebel CP, Ischiropoulos H, Bondy SC. Evaluation of the probe 2',7'-dichlorofluorescein as an indicator of reactive oxygen species formation and oxidative stress. *Chem Res Toxicol.* 1992;5:227–31.
- Bradford MM. Rapid and sensitive method for quantitation of microgram quantities of protein utilizing principle of protein-dye binding. *Anal Biochem.* 1976;72:248–54.
- Shilov IV, Seymour SL, Patel AA, Loboda A, Tang WH, Keating SP, et al. The paragon algorithm, a next generation search engine that uses sequence temperature values and feature probabilities to identify peptides from tandem mass spectra. *Mol Cell Proteom.* 2007;6:1638–55.
- Tian WN, Pignatari JN, Stanton RC. Signal-transduction proteins that associate with the platelet-derived growth-factor (Pdgf) receptor mediate the (Pdgf)-induced release of glucose-6-phosphate-dehydrogenase from permeabilized cells. *J Biol Chem.* 1994;269:14798–805.
- Tian WN, Braunstein LD, Pang JD, Stuhlmeier KM, Xi QC, Tian XN, et al. Importance of glucose-6-phosphate dehydrogenase activity for cell growth. *J Biol Chem.* 1998;273:10609–17.
- Yarian CS, Toroser D, Sohal RS. Aconitase is the main functional target of aging in the citric acid cycle of kidney mitochondria from mice. *Mech Ageing Dev.* 2006;127:79–84.
- Wu H, Xue RY, Tang ZQ, Deng CH, Liu TT, Zeng HZ, et al. Metabolomic investigation of gastric cancer tissue using gas chromatography/mass spectrometry. *Anal Bioanal Chem.* 2010;396:1385–95.
- Chen FF, Zhang JT, Song XS, Yang J, Li HP, Tang HR, et al. Combined metabolomic and quantitative real-time PCR analyses reveal systems metabolic changes of fusarium graminearum induced by Tri5 gene deletion. *J Proteom Res.* 2011;10:2273–85.
- Halket JM, Waterman D, Przyborowska AM, Patel RKP, Fraser PD, Bramley PM. Chemical derivatization and mass spectral libraries in metabolic profiling by GC/MS and LC/MS/MS. *J Exp Bot.* 2005;56:219–43.
- Wang L, Hou ET, Wang ZJ, Sun N, He LQ, Chen L, et al. Analysis of metabolites in plasma reveals distinct metabolic features between Dahl salt-sensitive rats and consomic SS.13(BN) rats. *Biochem Biophys Res Commun.* 2014;450:863–9.

23. Kanda A, Hashimoto H. Effects of semotiadil fumarate, a novel calcium-antagonist, on blood-pressure and heart-rate in conscious spontaneously hypertensive rats. *Jpn J Pharmacol*. 1993;63:121–4.
24. Wu JL, Wu QP, Huang JM, Chen R, Cai M, Tan JB. Effects of L-malate on physical stamina and activities of enzymes related to the malate-aspartate shuttle in liver of mice. *Physiol Res*. 2007;56:213–20.
25. Hou ET, Sun N, Zhang FC, Zhao CY, Usa K, Liang MY, et al. Malate and aspartate increase L-arginine and nitric oxide and attenuate hypertension. *Cell Rep*. 2017;19:1631–9.
26. Zheleznova NN, Yang C, Ryan RP, Halligan BD, Liang MY, Greene AS, et al. Mitochondrial proteomic analysis reveals deficiencies in oxygen utilization in medullary thick ascending limb of Henle in the Dahl salt-sensitive rat. *Physiol Genom*. 2012;44:829–42.
27. Raza H, Robin MA, Fang JK, Avadhani NG. Multiple isoforms of mitochondrial glutathione S-transferases and their differential induction under oxidative stress. *Biochem J*. 2002;366:45–55.
28. Schafer FQ, Buettner GR. Redox environment of the cell as viewed through the redox state of the glutathione disulfide/glutathione couple. *Free Radic Bio Med*. 2001;30:1191–212.
29. Lin MT, Beal MF. Mitochondrial dysfunction and oxidative stress in neurodegenerative diseases. *Nature*. 2006;443:787–95.
30. Siengdee P, Trakooljul N, Murani E, Schwerin M, Wimmers K, Ponsuksili S. MicroRNAs regulate cellular ATP levels by targeting mitochondrial energy metabolism genes during C2C12 myoblast differentiation. *PLoS ONE*. 2015;10:e0127850.
31. Schulte U, Fecke W, Krull C, Nehls U, Schmiede A, Schneider R, et al. In-Vivo dissection of the mitochondrial respiratory nadh-ubiquinone oxidoreductase (complex-I). *Biochim Biophys Acta Bioenerg*. 1994;1187:121–4.
32. Dunning CJR, McKenzie M, Sugiana C, Lazarou M, Silke J, Connelly A, et al. Human CIA30 is involved in the early assembly of mitochondrial complex I and mutations in its gene cause disease. *EMBO J*. 2007;26:3227–37.
33. Diaz F, Enriquez JA, Moraesa CT. Cells lacking Rieske iron-sulfur protein have a reactive oxygen species-associated decrease in respiratory complexes I and IV. *Mol Cell Biol*. 2012;32:415–29.
34. Kaludercic N, Giorgio V. The dual function of reactive oxygen/nitrogen species in bioenergetics and cell death: the role of ATP synthase. *Oxid Med Cell Longev*. 2016;2016:3869610.
35. Ni R, Zheng D, Xiong SD, Hill DJ, Sun T, Gardiner RB, et al. Mitochondrial calpain-1 disrupts ATP synthase and induces superoxide generation in type 1 diabetic hearts: a novel mechanism contributing to diabetic cardiomyopathy. *Diabetes*. 2016;65:255–68.
36. Taylor NE, Maier KG, Roman RJ, Cowley AW. NO synthase uncoupling in the kidney of Dahl S rats—role of dihydrobiopterin. *Hypertension*. 2006;48:1066–71.
37. Zheng L, Cardaci S, Jerby L, MacKenzie ED, Sciacovelli M, Johnson TI, et al. Fumarate induces redox-dependent senescence by modifying glutathione metabolism. *Nat Commun*. 2015;6:6001.